

# $\rho$ -meson properties at finite nuclear density\*

L.A. Kondratyuk<sup>1</sup>, A. Sibirtsev<sup>2</sup>, W. Cassing<sup>2</sup>  
Ye.S. Golubeva<sup>3</sup> and M. Effenberger<sup>2</sup>

<sup>1</sup> Institute of Theoretical and Experimental Physics,  
117259 Moscow, Russia

<sup>2</sup> Institute for Theoretical Physics,  
University of Giessen, D-35392 Giessen, Germany

<sup>3</sup> Institute of Nuclear Research,  
117312 Moscow, Russia

## Abstract

We calculate the momentum dependence of the  $\rho$ -meson selfenergy based on the dispersion relation for the  $\rho N$  scattering amplitude  $f(\omega)$  at low nuclear density. The imaginary part of  $f(\omega)$  is determined from the optical theorem, while the total  $\rho N$  cross section is obtained within the VDM at high energy and within the resonance model at low energy. Our numerical results indicate a sizeable broadening of the  $\rho$ -meson width in the medium especially for low relative momenta  $p$  while the real part of the  $\rho$  selfenergy is found to change its sign and to become repulsive already at momenta above 100 MeV/c. Extrapolating to nuclear saturation density  $\rho_0$  we find a dropping of the  $\rho$ -mass for  $p \approx 0$  roughly in line with the QCD sumrule analysis of Hatsuda while at high energy an increase of the  $\rho$ -mass close to the prediction by Eletsky and Joffe is obtained. However, when including a broadening of the baryonic resonances in the medium, the  $\rho$ -meson mass shift at  $p \approx 0$  becomes slightly repulsive whereas the width increases substantially.

PACS: 25.20.-x; 25.20.Dc; 25.40Ep

Keywords: Photonuclear reactions; Photon absorption and scattering; vector mesons; meson-nucleon interactions.

---

\*Supported by DFG, Forschungszentrum Jülich and BMBF.

# 1 Introduction

The properties of baryonic and mesonic resonances in the nuclear medium has received a vivid attention during the last years (cf. Refs. [1, 2, 3, 4, 5]) within the studies on the properties of hot and dense nuclear matter. Here, QCD inspired effective Lagrangian models [1, 4, 5] or approaches based on QCD sum rules [2, 3] predict that the masses of the vector mesons  $\rho$  and  $\omega$  should decrease with the nuclear density. On the other hand, with a dropping hadron mass the phase space for its decay decreases, which results in a modification of its width or lifetime in matter, while due to interactions with the surrounding nuclear medium the resonance width will increase [6, 7, 8, 9].

The in-medium properties of vector mesons have been addressed experimentally so far by dilepton measurements at the SPS, both for proton-nucleus and nucleus-nucleus collisions [10, 11, 12, 13]. As proposed by Li *et al.* [14], the enhancement in  $S + Au$  reactions compared to  $p + Au$  collisions in the invariant mass range  $0.3 \leq M \leq 0.7$  GeV might be due to a shift of the  $\rho$  meson mass. The microscopic transport studies in Refs. [15, 16, 17] for these systems point in the same direction, however, also more conventional selfenergy effects cannot be ruled out at the present stage [15, 18, 19, 20]. Especially the p-wave coupling of the  $\rho$ -meson to nucleons induces an attractive interaction at low relative momenta [20] which turns repulsive at large momenta. The explicit momentum dependence of the  $\rho$ -meson selfenergy thus is an important aspect to be investigated both, theoretically and experimentally e.g. by  $\pi^- A$  reactions [8, 9, 21, 22].

The main goal of this paper is to calculate the explicit momentum dependence of the  $\rho$ -meson potential at finite nuclear densities within a dispersive approach that is based on the resonance model at low relative momenta of the  $\rho$  with respect to the nucleon at rest and the vector dominance model at high relative momenta following the suggestion by Eletsky and Joffe [23]. Our work is organized as follows: In Section 2 we briefly recall the relation between hadron self energies and the hadron-nucleon scattering amplitude at low density and discuss the dominant interaction mechanisms. In Section 3 we present the related dispersion relations and evaluate the  $\rho N$  scattering amplitude from the  $\rho$ - photoproduction cross section at high energy. At low energy we use a resonance model to determine the  $\rho - N$  cross section. The implications for the real and imaginary part of the  $\rho$ -meson selfenergy at finite nuclear density are presented in Section 4 while a summary and discussion of open problems concludes this work in Section 5.

## 2 Hadronic resonances in the nuclear medium

The relativistic form of the wave equation describing the propagation of a mesonic resonance  $R$  in the nuclear matter is given as (see e.g. [9])

$$[-\nabla^2 + M_R^2 - iM_R\Gamma_R + U(\mathbf{r})] \Psi(\mathbf{r}) = E^2 \Psi(\mathbf{r}), \quad (1)$$

where  $E^2 = \mathbf{p}^2 + M_R^2$  and  $\mathbf{p}$ ,  $M_R$  and  $\Gamma_R$  are the momentum, mass and width of the resonance, respectively. The optical potential then is defined as

$$U(\mathbf{r}) = -4\pi f_{RN}(0) \rho_N(\mathbf{r}) \quad (2)$$

where  $f_{RN}(0)$  is the forward  $RN$ -scattering amplitude and  $\rho_N$  is the nuclear density.

It is useful to rewrite Eq. (1) in the form

$$[\nabla^2 + \mathbf{p}^2] \Psi(\mathbf{r}) = [U(\mathbf{r}) - \Delta] \Psi(\mathbf{r}), \quad (3)$$

where

$$\Delta = P^2 - M_R^2 - iM_R\Gamma_R \quad (4)$$

is the inverse resonance propagator in the vacuum. The four-momentum  $P$  in Eq. (4) can be defined through the four-momenta of the resonance decay products, i.e.

$$P = p_1 + p_2 + \dots \quad (5)$$

When the resonance decays inside the nucleus of radius  $R_A$  at density  $\rho_N$ , the propagator has the form

$$\Delta^* = \Delta + 4\pi f(0)\rho_N = P^2 - M_R^{*2} + iM_R^*\Gamma_R^* \quad (6)$$

where

$$M_R^{*2} = M_R^2 - 4\pi Re f(0)\rho_N, \quad (7)$$

$$M_R^*\Gamma_R^* = M_R\Gamma_R + 4\pi Im f(0)\rho_N. \quad (8)$$

Its spectral function then can be described (in a first approximation) by a Breit–Wigner formula (nonrelativistically) as

$$F(M) = \frac{1}{2\pi} \frac{\Gamma_R^*}{(M - M_R^*)^2 + \Gamma_R^{*2}/4}, \quad (9)$$

which contains the effects of collisional broadening,

$$\Gamma_R^* = \Gamma_R + \delta\Gamma \quad (10)$$

with

$$\delta\Gamma = \gamma v \sigma_{RN} \rho_N, \quad (11)$$

and a shift of the meson mass

$$M_R^* = M_R + \delta M_R \quad (12)$$

with

$$\delta M_R = -\gamma v \sigma_{RN} \rho_N \alpha. \quad (13)$$

In Eqs. (11),(13)  $v$  is the average resonance velocity with respect to the target at rest,  $\gamma$  is the associated Lorentz factor,  $\rho_N$  is the nuclear density while  $\sigma_{RN}$  is the resonance-nucleon total cross section and  $\alpha = Re f(0)/Im f(0)$ .

The sign of the resonance mass shift depends on the sign of the real part of the forward  $RN$  scattering amplitude which again depends on the momentum of the resonance. For example, at low momenta ( $p \approx 0$ ) various authors [1, 2, 3, 4] predict a decreasing mass of the vector mesons  $\rho$ ,  $\omega$  and  $\phi$  with the nucleon density, whereas Eletsky and Ioffe have argued recently [23] that the  $\rho$ -meson should become heavier

in nuclear matter at momenta of 2-7 GeV/c. If the ratio  $\alpha$  is small - which is actually the case for the reactions considered because many reaction channels are open - the broadening of the resonance will be the main effect. As it was shown in Ref. [24] the account of this effect can also essentially influence the predictions of QCD sum rules [2, 3]. Therefore it is useful to perform independent calculations for the real part of the  $\rho N$  forward scattering amplitude which can also be used at low momenta.

Whereas the  $\rho$ -meson spectral function in the nuclear medium has been evaluated in Refs. [5, 18, 19] in dynamical models by considering its  $2\pi$  decay mode and taking into account the rescattering of pions on nucleons in the medium, we here address an approach based on dispersion relations using experimental information on the vacuum scattering amplitude as input as well as on the  $\rho N$  couplings (cf. Ref. [25]). Another important point is that Eqs. (11) and (13) for the collisional broadening and mass shift are valid only at low densities when the resonance-nucleon scattering amplitude inside the nucleus is the same as in the vacuum. A discussion of this point will be presented in Section 3.2 explicitly.

### 3 The $\rho$ -nucleon scattering amplitude in vacuum

Within the framework of the Vector Dominance Model (VDM) the Compton scattering amplitude can be expressed through the  $\rho N$ ,  $\omega N$  and  $\phi N$  scattering amplitudes as

$$T_{\gamma N}(s, t) = \frac{e^2}{4\gamma_\rho^2} \left[ T_{\rho N}(s, t) + \frac{\gamma_\rho^2}{\gamma_\omega^2} T_{\omega N}(s, t) + \frac{\gamma_\rho^2}{\gamma_\phi^2} T_{\phi N}(s, t) \right], \quad (14)$$

where  $T_{VN}(s, t)$  is the invariant amplitude for the elastic scattering of the transverse polarized vector meson on the nucleon,  $e^2/4\pi$  is the fine-structure constant,  $T_{\gamma N}(s, t)$  is the invariant Compton scattering amplitude and  $\gamma_\rho^2/4\pi=0.55$  [26, 27, 28]. According to experimental data (cf. [29]) the last 2 terms on the r.h.s. of Eq. (14) including the  $\omega N$  and  $\phi N$  amplitudes can be neglected as compared to the first term. Then the  $\rho N$  scattering amplitude can be expressed directly through the Compton amplitude by multiplying the latter with  $4\gamma_\rho^2/e^2$ ; this approach has been adopted by Eletsky and Ioffe in Ref. [23]. We note, however, that the experimental Compton scattering amplitude also contains contributions from the continuum of  $2\pi$  and  $n\pi$  intermediate states at high energy such that Eq. (14) appears questionable. Here we will adopt the experimental results on  $\rho$ -photoproduction instead which are more closely related to the  $\rho$ -meson itself (cf. Section 3.1).

In general, the  $\rho N$  scattering amplitude  $f(\omega, \theta)$ , which enters into Eqs. (7),(8) for the resonance mass shift and collisional broadening can be expressed through the invariant scattering amplitude by

$$T_{\rho N}(s, t) = 8 \pi \sqrt{s} \frac{p_{cm}}{p_{lab}} f(\omega, \theta), \quad (15)$$

where  $p_{cm}$ ,  $p_{lab}$  are the momenta of the incident particle in the c.m. and laboratory systems, respectively, while  $\theta$  is the scattering angle in the laboratory frame. Furthermore, the real part of the forward  $\rho N$  scattering amplitude is related to its imaginary

part through the dispersion relation (cf. Ref. [30])

$$Ref(\omega) = Ref(\omega_0) + \frac{2(\omega^2 - \omega_0^2)}{\pi} P \int_{\omega_{min}}^{+\infty} \frac{d\omega' \omega' Imf(\omega')}{(\omega'^2 - \omega_0^2)(\omega'^2 - \omega^2)}, \quad (16)$$

where  $\omega = \omega_0$  is a subtraction point and  $\omega_{min}$  is the threshold energy. The imaginary part of the forward scattering amplitude  $Imf(\omega)$ , furthermore, is related to the total cross section by the optical theorem,

$$Imf(\omega) = \frac{p_{lab}}{4\pi} \sigma_{tot}(\omega). \quad (17)$$

Thus the knowledge of the total cross section  $\sigma_{tot}(\omega)$  is sufficient to determine  $Ref(\omega)$  through the dispersion relation (16) once the amplitude is known 'experimentally' at the subtraction point  $\omega_0$ .

### 3.1 The $\rho N$ total cross section from photoproduction

Within the VDM one can express the  $\rho N$  scattering amplitude not only through the Compton scattering amplitude (Eq. (14)) but also through the amplitude for  $\rho$ - photoproduction as:

$$T_{\rho N}(s, t) = \frac{2\gamma_\rho}{e} T_{\gamma N \rightarrow \rho N}(s, t). \quad (18)$$

Furthermore, the  $\rho N$  total cross section can be related to the differential cross section of the reaction  $\gamma p \rightarrow \rho p$  as

$$\sigma_{\rho p}^2 = \frac{\gamma_\rho^2}{4\pi} \frac{64\pi}{\alpha} \frac{1}{1 + \alpha_{\rho p}^2} \left( \frac{q_\gamma}{q_\rho} \right)^2 \frac{d\sigma_{\gamma p \rightarrow \rho p}}{dt} \Big|_{t=0}. \quad (19)$$

Here  $q_\gamma$  and  $q_\rho$  are the c.m. momenta of the  $\gamma N$  and  $\rho N$  systems at the same invariant collision energy  $\sqrt{s}$ . Furthermore, we assume that the ratio  $\alpha_{\rho p}$  of the real to imaginary part of the  $\rho N$  forward scattering amplitude is small. This assumption is valid at least for energies above 3 GeV [29]. Thus using the  $\rho$  photoproduction data from Refs. [26, 27, 28] the  $\rho N$  scattering amplitude is fixed at high energy.

We note that at higher energies one can calculate the total cross section of the  $\rho N$  interaction also within the Quark Model (QM), where  $\sigma_{\rho N}$  can be expressed in terms of pion-nucleon cross sections as

$$\sigma_{\rho^0 N} = \frac{1}{2} (\sigma_{\pi^- N} + \sigma_{\pi^+ N}), \quad (20)$$

while the  $\pi N$  cross sections can be taken from a Regge fit to the experimental data [31]. Though the additive quark model at first sight appears questionable for Goldstone bosons as the pions, the cross section  $\sigma_{\rho N}$  will turn out practically the same as in the VDM for  $\rho$ -meson momenta above 2 GeV/c (see below).

### 3.2 The resonance model combined with VDM

If the VDM would be valid at all energies we could calculate the mass shift and collisional broadening of the  $\rho$  meson in nuclear matter at low densities by inserting Eq. (18) in Eqs. (7) and (8) from Sect. 2. However, the VDM is expected to hold only at high energies  $\omega > 2$  GeV [32] since at lower energies ( $\omega \leq 1.5$  GeV) there are a lot of baryonic resonances which couple strongly to the transverse as well as to the longitudinal  $\rho$ -mesons [33]. Therefore at low energies it is necessary to describe the  $\rho N$  interaction within the framework of a resonance model [25, 34]. In the following we consider the  $\rho N$  forward scattering amplitude being averaged over the  $\rho$ -meson transverse and longitudinal polarizations.

Experimental information on the baryonic resonances and their coupling to the  $\rho$ -meson is available for masses below 2 GeV. We saturate the  $\rho N$  total cross section at low energies by the resonances listed in Table 1. For the Breit-Wigner contribution of each resonance we adopt the approach developed by Manley and Saleski [35]. In this model the total  $\rho N$  cross section is given as a function of the  $\rho$ -meson mass  $m$  and the invariant collision energy  $\sqrt{s}$  as:

$$\sigma_{\rho N}(m, \sqrt{s}) = \frac{2\pi}{3q_\rho^2} \sum_R (2J_R + 1) \frac{s \Gamma_{\rho N}^{in}(m, \sqrt{s}) \Gamma_{tot}(\sqrt{s})}{(s - M_R^2)^2 + s \Gamma_{tot}^2(\sqrt{s})}. \quad (21)$$

Here  $q_\rho$  denotes the c.m. momentum of the  $\rho N$  system,  $J_R$  the spin of the resonance,  $M_R$  the pole mass and  $\Gamma_{tot}$  the total width as a sum over the partial channels. For the case of an unstable particle in the final channel the partial width has to be integrated over the spectral function of this particle. The energy dependence of the partial width  $\Gamma_{\rho N}$  for the decay of each baryonic resonance into the  $\rho N$  channel, i.e.  $R \rightarrow \rho N$ , is given by

$$\Gamma_{\rho N}(\sqrt{s}) = \Gamma_{\rho N}(M_R) \frac{g(\sqrt{s})}{g(M_R)}, \quad (22)$$

where  $\Gamma_{\rho N}(M_R)$  is the  $\rho N$  partial width at the resonance pole  $M_R$ , while the function  $g(\sqrt{s})$  is determined as

$$g(\sqrt{s}) = \int_{2m_\pi}^{\sqrt{s}-m_N} A_\rho(m') \frac{q_{\rho N}(m')}{\sqrt{s}} B_l^2(q_{\rho N}) dm'. \quad (23)$$

In Eq. (23)  $q_{\rho N}(m')$  is the c.m. momentum of the nucleon and the  $\rho$ -meson with mass  $m'$ ,  $B_l$  is a Blatt–Weisskopf barrier penetration factor,  $l$  denotes the angular momentum of the  $\rho N$  system and  $A_\rho$  is the spectral function of the  $\rho$ -meson in free space taken as

$$A_\rho(m) = \frac{2}{\pi} \frac{m^2 \Gamma_\rho(m)}{(m^2 - M_\rho^2)^2 + m^2 \Gamma_\rho^2(m)}, \quad (24)$$

where  $M_\rho = 770$  MeV and the mass dependent width  $\Gamma_\rho(m)$  of the  $\rho$ -meson is given by

$$\Gamma_\rho(m) = \frac{\Gamma_\rho^0 M_\rho}{m} \left[ \frac{q_{\pi\pi}(m)}{q_{\pi\pi}(M_\rho)} \right]^3 \left[ \frac{1 + \delta^2 q_{\pi\pi}^2(M_\rho)}{1 + \delta^2 q_{\pi\pi}^2(m)} \right]^2 \quad (25)$$

with  $\delta = 5.3$  (GeV/c) $^{-1}$  and  $\Gamma_\rho^0 = 150$  MeV.

The incoming width in Eq. (21) reads:

$$\Gamma_{\rho N}^{in}(m, \sqrt{s}) = C_{\rho N}^{I_R} \frac{q_{\rho N}(m)}{\sqrt{s}} B_l^2(q_{\rho N}) \frac{\Gamma_{\rho N}(M_R)}{g(M_R)}, \quad (26)$$

where  $C_{\rho N}$  denotes the appropriate Clebsh-Gordan coefficient for the coupling of the isospins of  $\rho$  and nucleon to the isospin  $I_R$  of the resonance. The properties of the baryonic resonances coupled to the  $\rho$  are listed in Table 1; in the following calculations we exclude the resonances with only one star confidence level.

Within the resonance model we can evaluate the total  $\rho N$  cross section as the function of two variables: the  $\rho$  momentum and the invariant mass  $m$  of the  $\rho$ -meson. Fig. 1 shows the momentum dependence of the total  $\rho N$  cross section according to (21) for different masses of the  $\rho$ -meson, respectively. At higher momenta ( $p_\rho \geq 1.5$  GeV/c), where the total cross section is described by the VDM or the QM (20), respectively, we assume that it does no longer depend on  $m$ .

In Fig. 2 we present the prediction of the resonance model for the total  $\rho N$  cross section – averaged over the  $\rho$ -meson spectral function  $A_\rho$  – in comparison to the result from the quark-model (20) (QM, dashed line). The solid circles in Fig. 2 show the total  $\rho p$  cross section obtained by Eq. (19) and the experimental forward  $\rho$ -photoproduction data from [26, 27, 28]. Furthermore, the squares in Fig. 2 (for  $p_\rho \geq 10$  GeV/c) show the  $\rho N$  cross section extracted from the reaction  $\gamma + d \rightarrow \rho^0 + d$  independently of the VDM [36]. As mentioned before, the results for the total cross section of the  $\rho N$  interaction calculated within the framework of the quark-model (QM) and the VDM are in fair agreement at momenta above 2 GeV/c. The dotted line in Fig. 2 shows the interpolation between the low and high energy parts of the total  $\rho p$  cross section which we will adopt furtheron in Eq. (17).

In order to compute the real part of the amplitude we use the dispersion relation (16) and perform the subtraction at  $\omega_0 = 4.46$  GeV since at this energy  $Re f(\omega_0)$  was calculated with the VDM from the  $\rho$ -meson photoproduction differential cross section measured by DESY-MIT [37] and the Daresbury group [38]. We note that the VDM should be valid at the energy of 4.46 GeV such that the subtraction point is no hidden parameter in our approach. Since the resonance model is also valid below the  $\rho N$  threshold, the  $\rho$  contribution in this case is calculated as an integral over the available invariant mass of the  $2\pi$  system.

The real and imaginary parts of the  $f_{\rho N}$  amplitude - calculated with the total  $\rho N$  cross section averaged over the  $\rho$ -meson spectral function in free space (24) - are shown in Fig. 3. The imaginary part corresponds to the total  $\rho p$  cross section from Fig. 2 using the dashed line as an interpolation. Whereas the real part  $Re f_{\rho N}$  is negative at high momentum, it changes the sign at  $p_\rho \approx 100$  MeV/c. This behaviour of the real part for the  $f_{\rho N}$  amplitude has its origin in the resonance contribution at low energies. To illustrate this point we present in Fig. 4  $Re f_{\rho N}$  neglecting the part of the  $\rho N$  cross section from the resonance model. In fact, in this case the real part does not change its sign and remains negative over the whole momentum range.

Furthermore, Fig. 5 shows the real part of the forward  $\rho N$  scattering amplitude calculated for the different masses of the two-pion system  $m$  coupled to the  $\rho$ -meson. We find that  $Re f_{\rho N}$  substantially depends on the  $\rho$ -meson mass as well as on momentum.

Note that the dip for  $p_\rho \simeq 1$  GeV/c is due to our interpolation between the low and the high energy regions and thus an artefact of our model which should be discarded. We also have to mention that the magnitude of the  $\rho$ -meson momentum, where the real part of the forward  $\rho N$  scattering amplitude changes its sign, depends on the prescription for the transition between the resonance and high energy part of the total cross section, which is actually model dependent, and estimate this uncertainty as  $\delta p_\rho = \pm 30$  MeV/c.

## 4 Mass shift and broadening of the $\rho$ -meson in the nuclear medium

In the low density approximation one now can express the correction of the  $\rho$ -meson mass and width at finite nuclear density  $\rho_N$  through  $f_{\rho N}$  using Eqs. (7) and (8). We show the corresponding results for the mass and width of the  $\rho$ -meson in Fig. 6 calculated at saturation density  $\rho_0 \approx 0.16$  fm<sup>-3</sup> with the averaged  $\rho N$  cross section from the resonance model as described above. The upper part of Fig. 6 also shows the recent result from Hatsuda [39] calculated within the QCD sumrule approach at  $\omega = m_\rho$  by the full dot. Our result for  $\delta m$  in the low density approximation is in agreement with this calculation for  $p_\rho \approx 0$ . Note that the QCD sumrule analysis is also limited to low nuclear densities due to the unknown behaviour of the quark 4-point condensates in the medium. At high momenta  $p \geq 2$  GeV/c our result is also in qualitative agreement with the VDM predictions for the mass shift as found by Eletsky and Ioffe [23]. In their case the  $\rho$  mass shift increases from 60 MeV at  $p_\rho = 2$  GeV/c to 90 MeV at 7 GeV/c, whereas our analysis gives a shift of  $\simeq 70$  MeV at 2 GeV/c and  $\simeq 120$  MeV at 7 GeV/c. The deviations with the results from [23] are due to the use of the  $\rho$ -photoproduction amplitudes (19) instead of the Compton scattering amplitude (14) used by the latter authors.

Thus, if the low density approximation could be extrapolated up to  $\rho_0$ , our model would demonstrate that the repulsive interaction of the  $\rho$ -meson at high momenta might be consistent with an attractive  $\rho N$  interaction at low energies. However, as it was shown Ref. [24], the effect of the finite  $\rho$  width can essentially influence the predictions of QCD sum rules [2, 3]. Furthermore, recent microscopic calculations of the  $\rho$ -spectral function at low energies do not show any substantial attraction for slow  $\rho$ -mesons at normal nuclear density [5, 40].

It is thus important to check if the results obtained within the low density approximation are still valid at normal nuclear density  $\rho_0$ . Up to now in calculating the mass shift and broadening of the width for the  $\rho$ -meson (shown in Fig. 6) we have used the vacuum  $\rho N$  scattering amplitude with resonance contributions which, however, might be different in nuclear matter. An indication for a possible strong medium-modification of baryonic resonances is the experimental observation that the total photoabsorption cross section in nuclei for  $A \geq 12$  does not show any resonant structure except the  $\Delta(1232)$  isobar [41, 42, 43]. As was shown in Ref. [6, 44] this might be explained by a strong in-medium broadening of the  $D_{13}(1520)$  resonance ( $\Gamma_{med} \simeq 300$  MeV compared to the vacuum width  $\Gamma_R \simeq 120$  MeV), but not by conventional medium effects like



Fermi motion or Pauli blocking. While a collision broadening of this order is hard to justify, it might arise from the strong coupling of the  $D_{13}$  resonance to the  $\rho N$  channel and a medium modification of the  $\rho$ -meson [34]. Furthermore, in Ref. [40] it has been shown that such a mechanism can lead to an in-medium width of the  $D_{13}(1520)$  resonance of about 350 MeV.

To estimate how the latter effect influences our results we have performed also calculations for the in-medium  $\rho N$  total cross section by assuming that at normal nuclear density the widths of all resonances - coupled to the  $\rho N$  channel - are twice as in the vacuum, but their  $\rho N$  branching ratios stay the same. This in-medium  $\rho N$  cross section then was used in the dispersion relation for the calculation of the in-medium real part of the  $\rho N$  forward scattering amplitude.

The results of these calculations are shown in Fig. 7 for the total  $\rho\rho$  cross section and the real part of the forward scattering amplitude calculated with different widths of all baryonic resonances. The factor  $\kappa$  in Fig. 7 stands for the ratio of the in-medium width of the baryonic resonance to its value in free space. We see that the higher order resonance broadening effects have a strong influence on the  $\rho N$  scattering amplitude in the resonance region. The total cross section becomes smoother at low energy and as a result the real part of  $f_{\rho N}(0)$  does not change sign anymore with decreasing  $p_\rho$ . At small  $p_\rho$  it remains negative, which means that the main medium effect for the  $\rho$ -meson at normal nuclear density is the collisional broadening; the mass shift is slightly repulsive. This result is in qualitative agreement with recent calculations of the  $\rho$ -meson spectral function at low energies from Refs. [5, 18, 40]. However, a note of caution has to be added here because the predictions within the resonance model are only of qualitative nature. The properties of nuclear resonances as well as their branching to the  $\rho$  channel in the dense medium are unknown so far. Furthermore, the influence of exchange-current corrections at high density on the  $\rho$  meson properties should be considered as well.

## 5 Conclusions

In summary, we have calculated the momentum dependence of the  $\rho$ -meson selfenergy (or in-medium properties) based on the dispersion relation (16) for the  $\rho N$  scattering amplitude at finite (but small) nuclear density. The imaginary part of  $f(\omega)$  is calculated via the optical theorem (17) while the total  $\rho N$  cross section is obtained within the VDM at high energy and within the resonance model at low energy. The scattering amplitude  $f(\omega)$  thus is entirely based on experimental data. Our numerical results indicate a sizeable broadening of the  $\rho$ -meson width in the medium especially for low relative momenta  $p_\rho$ . In the low density approximation the real part of its selfenergy is found to be attractive for  $p_\rho \leq 100$  MeV/c and to change its sign, becoming repulsive at higher momenta in line with the prediction by Eletsky and Joffe [23]. Extrapolating the low density approximation to nuclear saturation density we obtain a dropping of the  $\rho$ -mass at  $p_\rho \approx 0$  in line with the QCD sumrule analysis of Hatsuda [39]. Thus our dispersion approach demonstrates that the results of Refs. [23] and Ref. [39] do not contradict each other due to the rather strong momentum dependence of the  $\rho N$  scattering amplitude.

However, the resonance part of the  $\rho N$  scattering amplitude is also influenced by the nuclear medium at saturation density such that the moderate attraction at  $p_\rho \simeq 0$  changes to a small repulsion. This behaviour of the  $\rho$ -meson selfenergy is in qualitative agreement with the recent microscopic calculations of Rapp, Chanfray and Wambach [18, 19] as well as Klingl et al. [5] for the  $\rho$  spectral function. In the latter case the  $\rho$ -meson essentially broadens significantly in the dense medium which implies lifetimes of the  $\rho$ -meson less than 1 fm/c already at density  $\rho_0$ ; in simple words: according to our dispersion approach the  $\rho$ -meson 'melts' at high nuclear density and does not 'drop in mass' as suggested by the scaling hypothesis of Ref. [1].

We, finally, note that the explicit momentum dependence of the  $\rho$ -meson selfenergy is also an important issue that has to be incorporated e.g. in transport theories that attempt to extract information on the  $\rho$  spectral function in comparison to experimental dilepton data.

The authors acknowledge many helpful discussions with K. Boreskov, E.L. Bratkovskaya, B.L. Ioffe, U. Mosel and Yu. Simonov throughout this study.

## References

- [1] G. Brown and M. Rho, Phys. Rev. Lett. **66**, 2720 (1991).
- [2] T. Hatsuda and S. Lee, Phys. Rev. C **46**, R34 (1992).
- [3] M. Asakawa and C.M. Ko, Phys. Rev. C **48**, R526 (1993).
- [4] C.M. Shakin and W.-D. Sun, Phys. Rev. C **49**, 1185 (1994).
- [5] F. Klingl and W. Weise, Nucl. Phys. **A606**, 329 (1996); F. Klingl, N. Kaiser, and W. Weise, Nucl. Phys. **A617**, 449 (1997); *ibid.* **A624**, 927 (1997) .
- [6] L. A. Kondratyuk, M. Krivoruchenko, N. Bianchi, E. De Sanctis, and V. Muccifora, Nucl. Phys. **A579**, 453 (1994).
- [7] K.G. Boreskov, J. Koch, L.A. Kondratyuk, and M.I. Krivoruchenko, Phys. of Atomic Nuclei **59**, 1908 (1996); K.G. Boreskov, L.A. Kondratyuk, M.I. Krivoruchenko, and J. Koch Nucl. Phys. **A619** , 295 (1997).
- [8] W. Cassing, Ye.S. Golubeva, A.S. Iljinov, and L.A. Kondratyuk, Phys. Lett. B **396**, 26 (1997).
- [9] Ye.S. Golubeva, L.A. Kondratyuk, and W. Cassing, Nucl. Phys. **A625**, 832 (1997).
- [10] G. Agakichiev et al., Phys. Rev. Lett. **75**, 1272 (1995).
- [11] M.A. Mazzoni, Nucl. Phys. **A566**, 95c (1994).
- [12] T. Åkesson et al., Z. Phys. C **68**, 47 (1995).

- [13] A. Drees, Nucl. Phys. **A610**, 536c (1996).
- [14] G.Q. Li, C.M. Ko, and G.E. Brown, Phys. Rev. Lett. **75**, 4007 (1995).
- [15] W. Cassing, W. Ehehalt, and C.M. Ko, Phys. Lett. B **363**, 35 (1995).
- [16] W. Cassing, W. Ehehalt, and I. Kralik, Phys. Lett. B **377**, 5 (1996).
- [17] E. L. Bratkovskaya and W. Cassing, Nucl. Phys. **A619**, 413 (1997).
- [18] R. Rapp, G. Chanfray, and J. Wambach, Phys. Rev. Lett. **76**, 368 (1996).
- [19] R. Rapp, G. Chanfray, and J. Wambach, Nucl. Phys. **A617**, 472 (1997).
- [20] B. Friman and H.J. Pirner, Nucl. Phys. **A617**, 496 (1997).
- [21] W. Schön, H. Bokemeyer, W. Koenig, and V. Metag, Acta Physica Polonica B **27**, 2959 (1996).
- [22] Th. Weidmann, E.L. Bratkovskaya, W. Cassing, and U. Mosel, nucl-th/971104.
- [23] V.L. Eletsky and B.L. Ioffe, Phys. Rev. Lett. **78**, 1010 (1997).
- [24] S. Leupold, W. Peters, and U. Mosel, Nucl. Phys. **A 628**, 311 (1998).
- [25] A. Sibirtsev and W. Cassing, Nucl. Phys. **A 629**, 707 (1998).
- [26] R. Anderson, D. Gustavson, J. Johnson, D. Ritson, B.H. Wiik, W.G. Jones, D. Kreinick, F. Murphy, and R. Weinstein, Phys. Rev. D **1**, 27 (1970).
- [27] J. Ballam et al., Phys. Rev. D **7**, 3150 (1973).
- [28] R.M. Egloff et al., Phys. Rev. Lett. **43**, 657 (1979).
- [29] T.H. Bauer, R.D. Spital, D.R. Yennie, and F.M. Pipkin, Rev. Mod. Phys. **50**, 261 (1978).
- [30] J.D. Bjorken and S.D. Drell, Relativistic Quantum Fields, McGraw-Hill (1965) 209.
- [31] A. Donnachie and P.V. Landshoff., Phys. Lett.
- [32] B.L. Ioffe, V.A. Khoze, and L.N. Lipatov, Hard Processes (North-Holland, Amsterdam, 1984) Vol. 1.
- [33] Particle Data Group, Phys. Rev. D **54**, 1 (1996).
- [34] M. Effenberger, A. Hombach, S. Teis, and U. Mosel, Nucl. Phys. **A613**, 353 (1997); **A614**, 501 (1997).
- [35] D.M. Manley and E.M. Saleski, Phys. Rev. D **45**, 4002 (1992).

- [36] R.L. Anderson, D. Gustavson, J. Johnson, I. Overman, D.M. Ritson, and B.H. Wiik, Phys. Rev. D **4**, 3245 (1971).
- [37] H. Alvensleben et al., Phys. Rev. Lett. **25**, 1377 (1970); Phys. Rev. Lett. **27**, 444 (1971).
- [38] P.J. Biggs, D.W. Braben, R.W. Clift, E. Gabathuler, and R.E. Rand, Phys. Rev. Lett. **27**, 1157 (1971).
- [39] T. Hatsuda, nucl-th/9702002.
- [40] W. Peters, M. Post, H. Lenske, S. Leupold, and U. Mosel, Nucl. Phys. A **632**, 109 (1998).
- [41] N. Bianchi et al., Phys. Lett. B **299**, 219 (1993); Phys. Lett. B **309**, 5 (1993); Phys. Lett. B **325**, 333 (1994); M. Anghinolfi et al., Phys. Rev. C **47**, R922 (1993).
- [42] N. Bianchi et al., Phys. Rev. C **54**, 1688 (1996).
- [43] Th. Frommhold, F. Steiper, W. Henkel, U. Kneissl, J. Ahrens, R. Beck, J. Peise, and M. Schmitz, Phys. Lett. B **295**, 28 (1992).
- [44] S. Boffi, Y. Golubeva, L.A. Kondratyuk, M.I. Krivoruchenko, and E. Perazzi, Phys. Atom. Nucl. **60**, 1193 (1997).

Table 1: Properties of baryonic resonances coupled to the  $\rho$ -meson;  $l$  denotes the angular momentum of the  $\rho$  meson while the stars indicate the confidence level. In our calculations we discard resonances with only one star C.L.

Resonance	$J_R$	$M_R$ (MeV)	$\Gamma_R$ (MeV)	$l$	$\rightarrow N\rho$ (%)	C.L.
$S_{11}(1650)$	1/2	1659	173	0	3	* * *
$S_{11}(2090)$	1/2	1928	414	0	49	*
$D_{13}(1520)$	3/2	1524	124	0	21	* * *
$D_{13}(1700)$	3/2	1737	249	0	13	* * *
$D_{13}(2080)$	3/2	1804	447	0	26	**
$G_{17}(2190)$	7/2	2127	547	2	29	* * *
$P_{11}(1710)$	1/2	1717	478	1	3	* * *
$P_{11}(2100)$	1/2	1885	113	1	27	*
$P_{13}(1720)$	3/2	1717	383	1	87	* * *
$P_{13}$	3/2	1879	498	1	44	
$F_{15}(1680)$	5/2	1684	139	1	5	* * *
$F_{15}(1680)$	5/2	1684	139	3	2	* * *
$F_{15}(2000)$	5/2	1903	494	1	60	**
$F_{15}(2000)$	5/2	1903	494	3	15	**
$S_{31}(1620)$	1/2	1672	154	0	29	* * *
$S_{31}(1900)$	1/2	1920	263	0	38	* * *
$D_{33}(1700)$	3/2	1762	599	0	8	* * *
$D_{33}(1940)$	3/2	2057	460	0	35	*
$P_{31}(1910)$	1/2	1882	239	1	10	* * *
$F_{35}(1905)$	5/2	1881	327	1	86	* * *
$F_{35}$	5/2	1752	251	1	22	

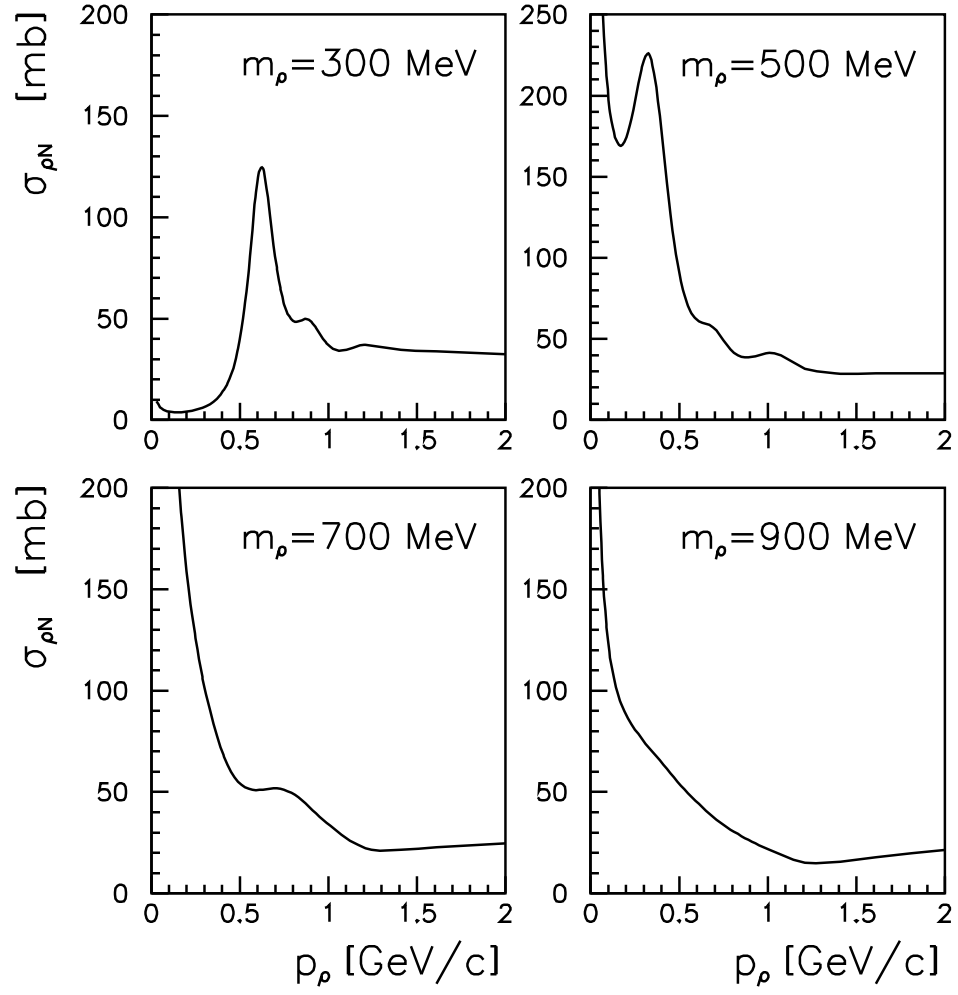


Figure 1: The total  $\rho N$  cross section for different invariant masses of the  $\rho$ -meson. At low energy the cross section was obtained within the resonance model while at high energies it was extrapolated from the quark model (QM) (20).

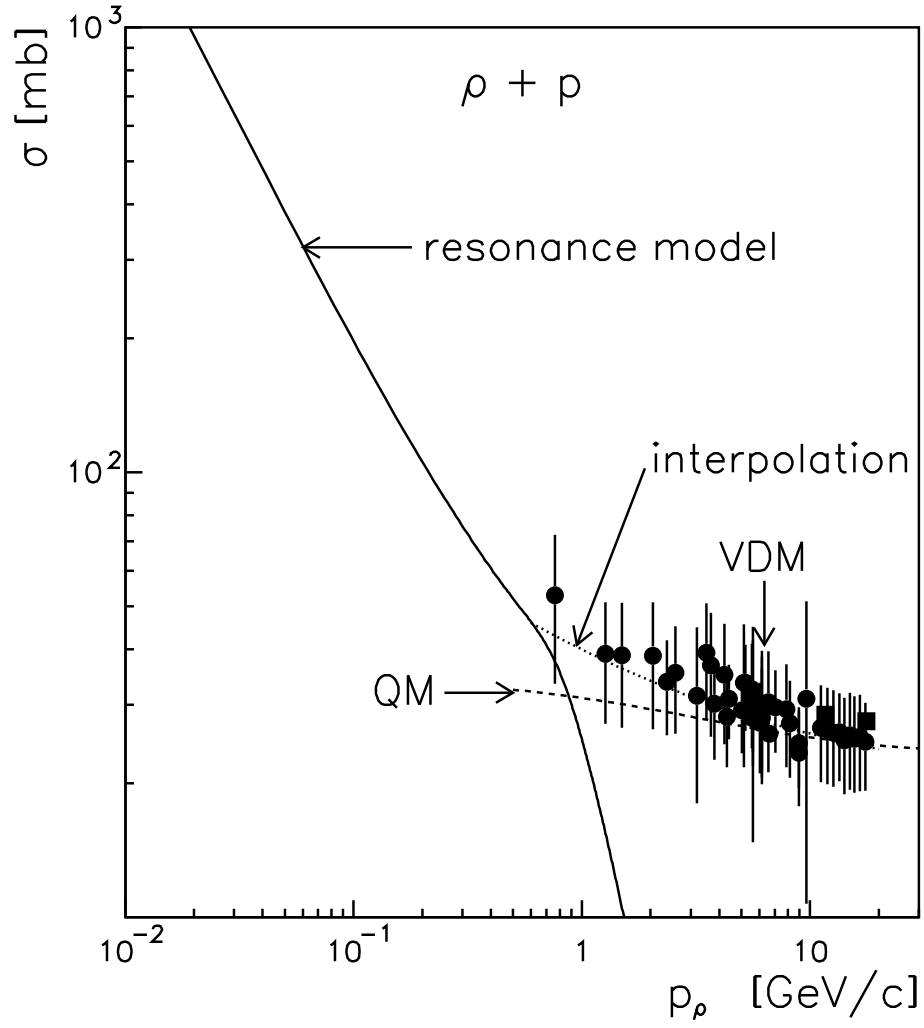


Figure 2: The total  $\rho p$  cross section. The solid line shows our calculation within the resonance model (21) while the dashed line is the result from the quark model (QM) (20). The full circles show the experimental data extracted from  $\rho$ -photoproduction while the squares are from [36]. The dotted line indicates the interpolation that will be used furtheron.

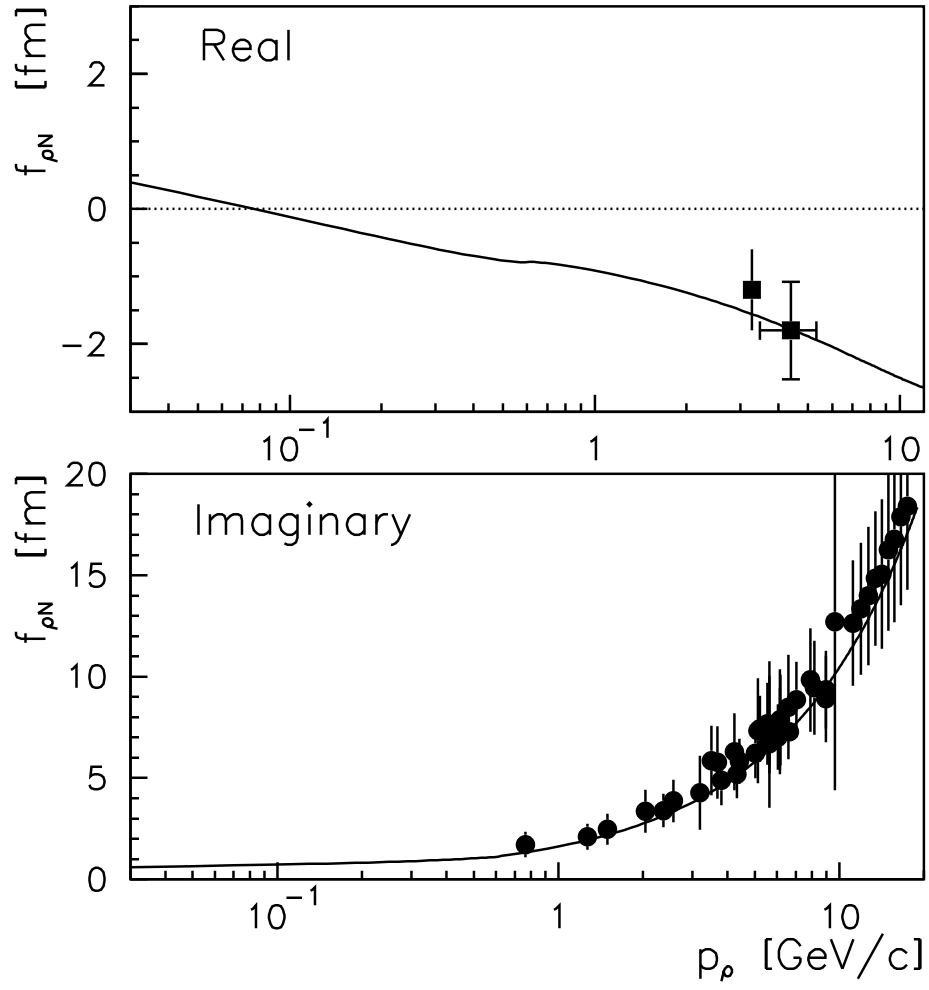


Figure 3: Real and imaginary part of the  $\rho N$  scattering amplitude in free space from the calculations (solid lines). The circles and squares are the results evaluated from the experimental data for  $\rho$ -meson photoproduction.



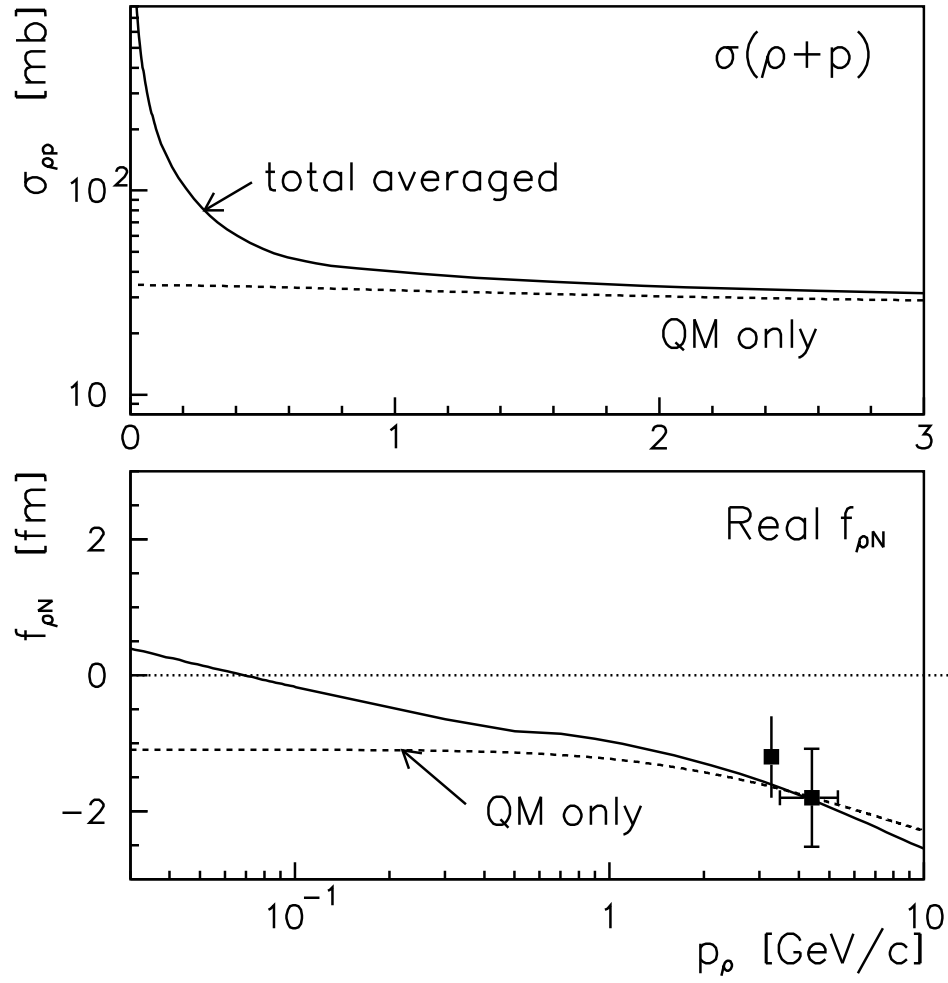


Figure 4: The total  $\rho p$  cross section and the real part of the  $\rho N$  scattering amplitude in free space as a function of the momentum  $p_\rho$ . The solid lines show our calculations with the total  $\rho N$  cross section while the dashed lines indicate the results with the cross section from the quark model (20), only. The squares are evaluated from the experimental data for  $\rho$ -meson photoproduction.

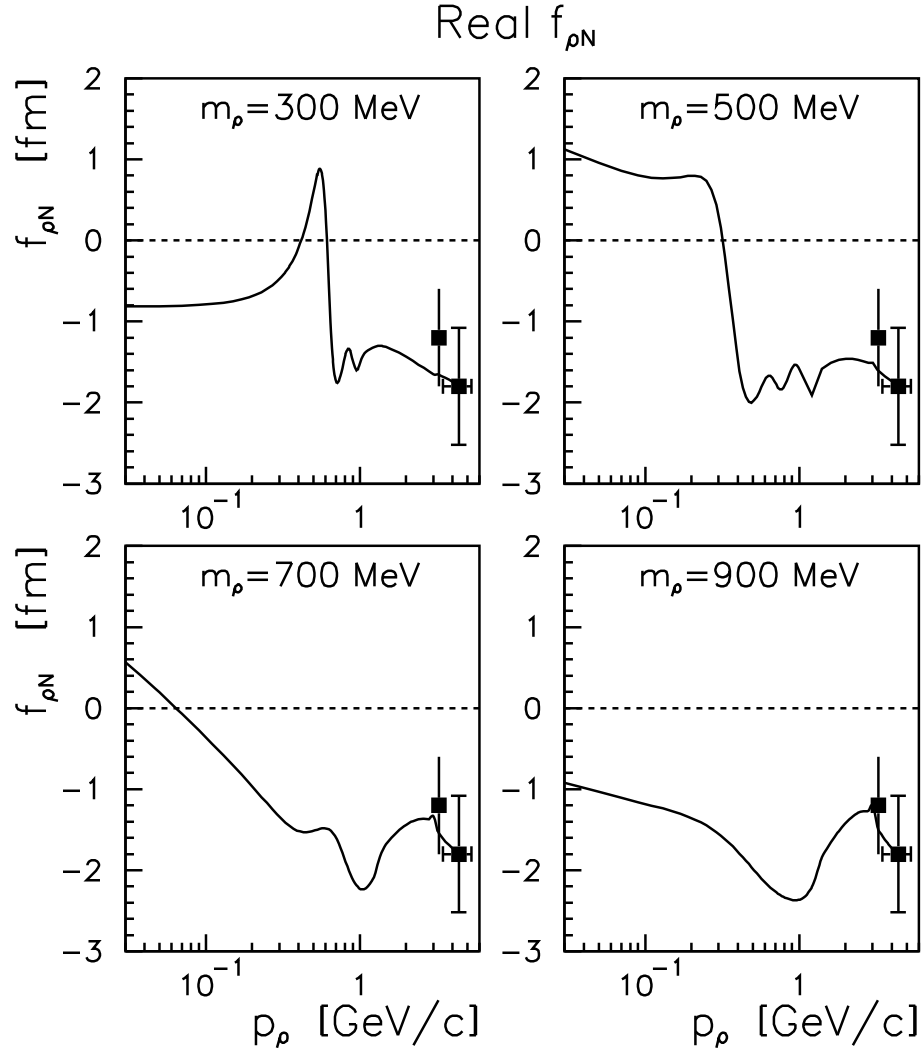


Figure 5: The real part of the  $\rho N$  scattering amplitude in free space calculated for different masses of the  $\rho$ -meson. The squares are evaluated from the experimental data for  $\rho$ -meson photoproduction.

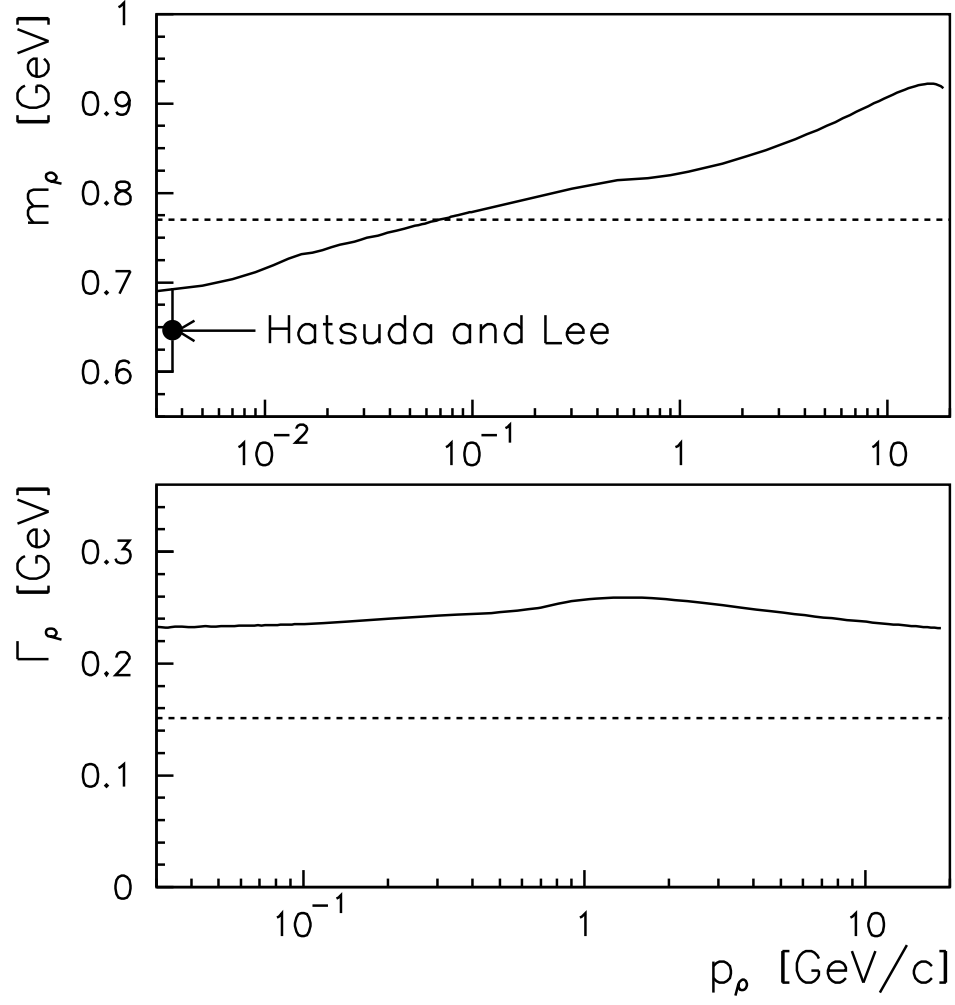


Figure 6: Mass and width of the  $\rho$ -meson at  $\rho_N = 0.16 \text{ fm}^{-3}$  according to our model in the low density approximation. The full dot corresponds to the result from Hatsuda [39] within the QCD sumrule approach.

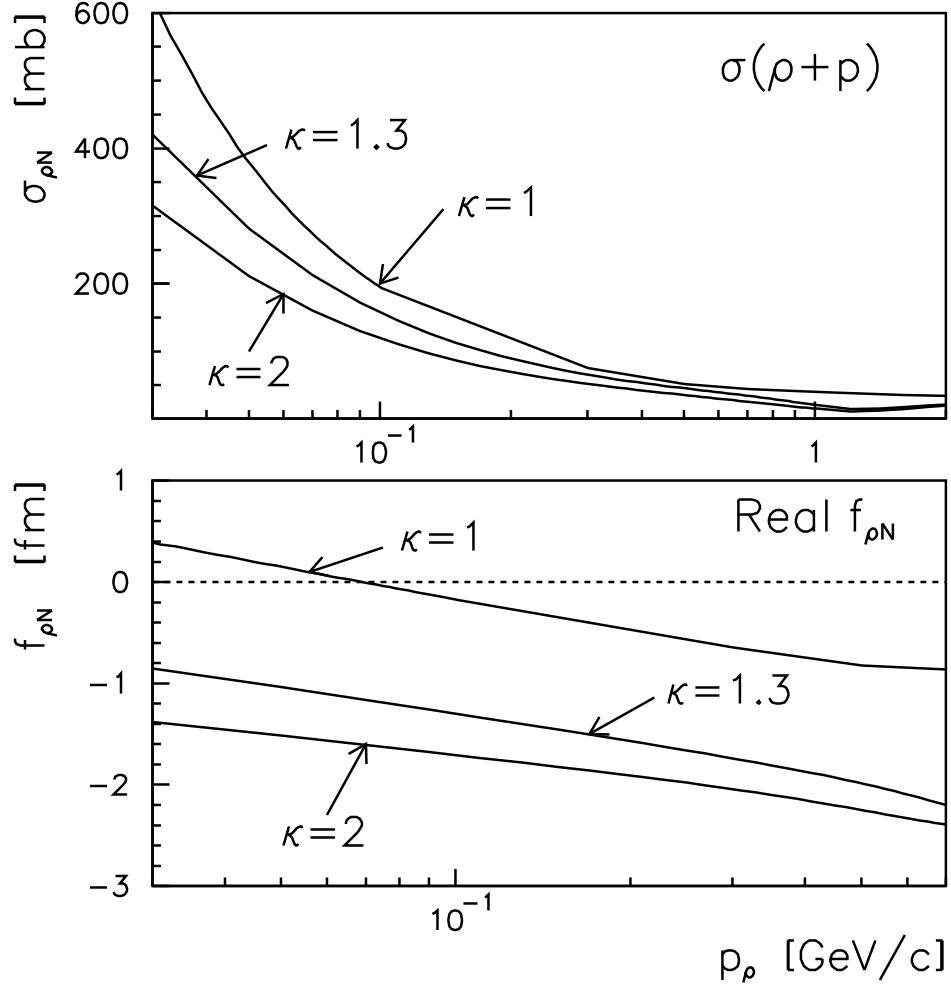


Figure 7: The total  $\rho N$  cross section and the real part of the  $\rho N$  scattering amplitude calculated for different widths of the baryonic resonances. The factor  $\kappa$  indicates the ratio of the in-medium resonance width to its vacuum width.